International Journal of Solids and Structures 125 (2017) 172–183

Contents lists available at ScienceDirect

International Journal of Solids and Structures

journal homepage: www.elsevier.com/locate/ijsolstr

Analysis of two-dimensional contact problems considering surface effect

Ning Jia[a,e], Yin Yao[b,c], Yazheng Yang[b,c,d], Shaohua Chen[b,c,d,*]

[a] LNM, Institute of Mechanics, Chinese Academy of Sciences, Beijing, 100190, China
[b] Institute of Advanced Structure Technology, Beijing Institute of Technology, Beijing, 100081, China
[c] Beijing Key Laboratory of Lightweight Multi-functional Composite Materials and Structures, Beijing Institute of Technology, Beijing, 100081, China
[d] Collaborative Innovation Center of Electric Vehicles in Beijing, Beijing Institute of Technology, Beijing, 100081, China
[e] School of Engineering Sciences, University of Chinese Academy of Sciences, Beijing, 100049, China

ARTICLE INFO

Article history:
Received 9 March 2017
Revised 26 June 2017
Available online 4 July 2017

Keywords:
Plane strain contact model
Surface energy density
Surface effect
Contact behavior
Nano-indentation hardness

ABSTRACT

Two-dimensional contact problems including a Boussinesq model, a semi-infinite substrate punched by a rigid flat-ended indenter or a cylindrical one, are systematically investigated with a recently developed continuum theory, in which surface effect on mechanical properties of materials is considered based on the concept of surface energy density. The contact stress and displacement fields are analyzed. It is found that the surface energy density of the indented bulk substrate, as only one additional parameter, serves as an important factor to influence the contact properties in contrast to the classical contact models. All the results show that the semi-infinite substrate becomes hardened when the surface effect is considered. Scaling analysis further demonstrates that differences between the theoretical predictions with surface effect and the classical contact solutions without surface effect become significant only if the contact width is comparable with the ratio of the bulk surface energy density to the bulk shear modulus. Specially, in the two-dimensional cylindrical punch problem, the smaller the punch size or the external compressive load, the more serious the deviation of the nano-indentation hardness predicted by the theoretical model with surface effect and the classical contact one. The results should be helpful not only for precise measurement of nano-indentation hardness but also for accurate evaluation of service performance of nanomaterials and nano-devices.

1. Introduction

Micro- and nano-indentation tests have been widely adopted in recent decades as one of the major techniques for measuring mechanical properties (hardness, elastic modulus, yield stress, etc.) of advanced materials such as crystalline solids, electromechanically intelligent materials and biomaterials with complex microstructures, etc. (Zhang and Xu, 2002; Rar et al., 2006; Li et al., 2007). The indentation size effect (ISE) has been reported as the indentation hardness inversely proportional to the micro- or nano-indentation depth (Gerberich et al., 2002; Feng and Nix, 2004).

In micrometer scale, the ISE was believed to arise essentially from the geometrically necessary dislocations associated with the non-uniform plastic deformation under indenters (Fleck et al., 1994; Voyiadjis and Al-Rub, 2005). As a result, many representative strain gradient plasticity theory were developed, in which intrinsic length parameters are involved in the constitutive relations (Nix and Gao, 1998; Chen and Wang, 2000, 2002; Huang et al., 2006). When the indenter size or indentation depth shrinks to a nanometer scale, the surface effect induced by a large surface-to-volume ratio of the contact zone becomes a crucial or even dominant factor responsible for the ISE, which is usually addressed as size effect in nanoscales (Gerberich et al., 2002). Nano-indentation hardness as a function of the surface energy density or surface stress was empirically derived by fitting experimental data of hardness (Gerberich et al., 2002; Zhang and Xu, 2002), which proves the prominent role of surface effect in nanoscale contact problems. Such a surface effect cannot be predicted within the framework of the classical contact mechanics (Johnson, 1987).

The developed surface elasticity theory in 1970s returns to the researcher's perspective, which now has been extensively developed and widely used as a feasible theoretical approach to account for the surface effect in nanomaterials and nanostructures (Gurtin and Murdoch, 1975, 1978). The main difference between the surface elasticity theory and the classical continuum one is the modified stress boundary condition, where a surface-induced traction as

* Corresponding author at: Beijing Institute of Technology, Zhongguancun South Street, Beijing, 100081, China.
E-mail addresses: chenshaohua72@hotmail.com, shchen@bit.edu.cn (S. Chen).

http://dx.doi.org/10.1016/j.ijsolstr.2017.07.007
0020-7683/

a function of the surface stress was introduced (Chen et al., 2006). A linearly elastic constitutive relation was assumed to describe the relationship between the surface stress and surface strain.

Besides the pioneering works of Gurtin and Murdoch (G-M model) (1975, 1978), lots of important progresses have been made in the field of surface effect in nanomaterials. Based on the G-M model, Steigmann and Ogden (1997) and Chhapadia et al. (2011) introduced a surface flexural stiffness into the constitutive relation, in order to characterize the curvature-dependence of surface energy under a bending or wrinkling conditions. Huang and Wang (2006, 2010), Huang and Sun (2007), Huang (2010) proposed a hyperelastic model within the framework of finite deformation theory, in which the Lagrangian and Eulerian formulations of the surface energy density depending on the residual surface stress were well achieved. The residual elastic field in the bulk part of a nanomaterial was further included in Huang and Wang (2013). Inspired by the above researches, Gao et al. (2014b; 2017) developed a comprehensive finite deformation theory, in which both the curvature-dependence of interface energy and the interface and bulk residual elastic fields were considered. With the surface elasticity theory and its extension, many problems related to nanoscale were investigated, for examples, size-dependent elastic behaviors of nano-wires, nano-particles, as well as nano-films were studied (He and Lilley, 2008; Wang and Feng, 2009; Li et al., 2011).

Recently, the surface elasticity theory has also been extended to analyze the nanoscale elastic contact problem, based on which a surface-induced traction in terms of surface stress is introduced into the stress boundary condition at the contact surface. Analytical models can be generally categorized into two groups according to the constitutive formulation of surface stress. One is to directly let the surface stress equal to the surface residual one (induced by surface relaxation), i.e., $\boldsymbol{\sigma}_s = \tau_0 \boldsymbol{I}$, where $\boldsymbol{\sigma}_s$, τ_0 and $\boldsymbol{I}$ are surface stress tensor, surface residual stress and unit tensor, respectively (Hajji, 1978; Koguchi, 1996, 2008; Long et al., 2012). Another is to consider the surface residual stress and surface deformation induced by the external load simultaneously, i.e., $\boldsymbol{\sigma}_s = \tau_0 \boldsymbol{I} + \boldsymbol{C}_s : \boldsymbol{\varepsilon}_s$, where $\boldsymbol{C}_s$ and $\boldsymbol{\varepsilon}_s$ denote the surface elastic constant and surface strain tensors, respectively (Zhao and Rajapakse, 2009; Gao et al., 2013; Zhou and Gao, 2013). A common finding is that the surface residual stress serving as a pre-stress on the contact surface yields relatively smooth distributions of the normal displacement and stress on the contact surface. The latter also reveals a dominant role of surface elasticity in affecting the shear stress at the contact surface.

Either the surface residual stress (surface tension) or the surface elastic constants were naturally introduced in the stress boundary conditions at the contact surface, both of which, however, are still difficult to determine experimentally till now. All the data used in theoretical analysis were mainly provided by molecular dynamics (MD) simulations (Miller and Shenoy, 2000; Shenoy, 2005; Mi et al., 2008) or taken arbitrarily. Even for MD simulation, many influence factors cannot be avoided in order to find the surface elastic constants or surface residual stress, for example, the selection of a proper atomic potential, the size of numerical model, how many atom layers forming the surface of nanomaterials. Furthermore, for the case of a semi-infinite elastic substrate, whether the effect of surface residual stress induced by surface relaxation on the contact behavior is obvious or not.

Another problem in the study of Hertzian contact problems with surface effect is that most models directly adopted the elliptical function given by the classical contact mechanics (Johnson, 1987) to describe the distribution of normal pressure at the contact area (Gao et al., 2013; Zhou and Gao, 2013). As we know that the normal pressure should be a result yielded by boundary value solution of elastic problems. The surface-induced traction as an additional boundary condition would affect the distribution of normal pressure in contact problems with surface effect. Fortunately, considering the effect of surface residual stress, (Long et al., 2012) has noted this issue and predicted a non-zero normal pressure at the contact fringe in contrast to a vanishing one in the classical contact mechanics (Johnson, 1987). Precise analysis of the Hertzian contact behavior with surface effect still lacks. It is worth noting that the adhesive interaction between two nano-sized elastic solids is another important factor that would affect the contact behavior. Some researchers have carried out studies based on the surface elasticity theory and its extensions (Gao et al., 2014a; Long et al., 2016).

In order to avoid the introduction of surface elastic constants, Chen and Yao (2014) developed a new elastic theory for nanomaterials recently. Since the surface energy density is an accepted parameter to characterize a surface, the surface-induced traction as a function of the surface energy density is well expressed from an atomistic viewpoint for nanomaterials, instead of the relation with the surface stress. As a result, the surface elastic constants are avoided. The mechanical properties of several typical nanostructures have been effectively studied based on the concept of surface energy density (Yao and Chen, 2015; Yao et al., 2015; Yao and Chen, 2016a, b; Yao et al., 2017).

In this paper, two-dimensional contact problems are investigated with the developed elastic theory for nanomaterials, where the surface effect is characterized by the surface energy density. One is the plane strain Boussinesq problem and the other two are a semi-infinite elastic substrate punched by a flat-tip indenter and a cylindrical one. Stress boundary conditions at the contact surface are formulated, in which the surface energy density is involved. General solutions of the contact stress and displacement are achieved and analyzed for three contact models, in which surface effect on the elastic contact behaviors can be clearly elucidated. The size effect of nano-indentation hardness is further discussed.

2. Brief introduction of the theory based on surface energy density

An elastic theory for nanomaterials was developed by Chen and Yao (2014), which is based on the surface energy density of nanomaterials. Consider a nano-solid with an idealized crystal structure in an initial (or reference) configuration. A Lagrangian coordinate system is imbedded in the crystal surface with two principal axes 1 and 2 parallel to the two basic vectors of a surface unit cell as shown in Fig. 1. a_{01}, a_{02} represent the initial lattice lengths in the two principal directions, respectively. Due to spontaneous surface relaxation, the lattice lengths become a_{r1} and a_{r2}, and further become a_1 and a_2 in the current configuration when subjected to an external loading. β denotes an angle between the two basic vectors.

The potential energy function Π of the nano-solid in the current configuration can be written as

$$\Pi(\boldsymbol{u}) = \int_{V-S} \psi(\boldsymbol{\varepsilon}) dV + \int_S \phi(\boldsymbol{\varepsilon}_s) dS - \int_{V-S} \boldsymbol{f} \cdot \boldsymbol{u} dV - \int_{S_p} \boldsymbol{p} \cdot \boldsymbol{u} dS \tag{1}$$

where ψ is the elastic strain energy density, ϕ is the Eulerian surface energy density in the current configuration, $\boldsymbol{f}$ and $\boldsymbol{p}$ are the body force and external surface traction, respectively. $\boldsymbol{u}$, $\boldsymbol{\varepsilon}$ and $\boldsymbol{\varepsilon}_s$ denote the displacement, strain and surface strain, respectively.

Variation analysis of Eq. (1) yields the following equilibrium equations and stress boundary conditions:

$$\begin{cases} \boldsymbol{\sigma} \cdot \nabla + \boldsymbol{f} = 0 (\text{in } V - S) \\ \boldsymbol{n} \cdot \boldsymbol{\sigma} \cdot \boldsymbol{n} = \boldsymbol{p} \cdot \boldsymbol{n} - \gamma_n \boldsymbol{n} (\text{on } S) \\ (\boldsymbol{I} - \boldsymbol{n} \otimes \boldsymbol{n}) \cdot \boldsymbol{\sigma} \cdot \boldsymbol{n} = (\boldsymbol{I} - \boldsymbol{n} \otimes \boldsymbol{n}) \cdot \boldsymbol{p} - \gamma_t (\text{on } S) \end{cases} \tag{2}$$

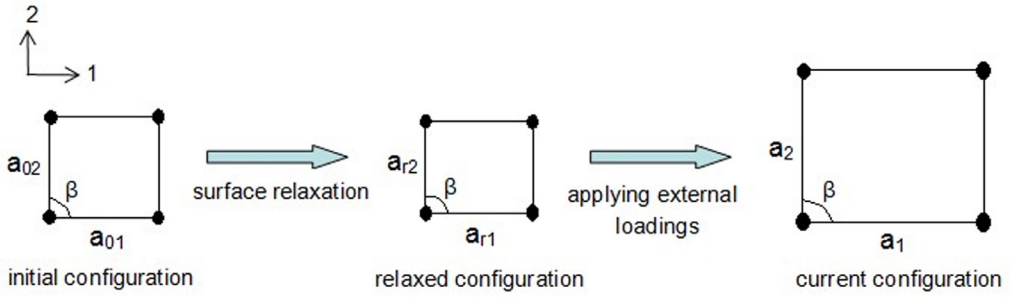

Fig. 1. Schematic of a surface unit cell in the initial (reference), relaxed and current configurations.

where $\boldsymbol{\sigma}$ is the bulk Cauchy stress tensor, $\boldsymbol{n}$ is the unit normal vector perpendicular to the boundary surface S of the nano-solid, $\mathbf{I}$ is a unit tensor; γ_n and $\boldsymbol{\gamma}_t$ are the normal and tangential components of an additional surface-induced traction vector $\boldsymbol{\gamma}$, respectively, which is similar to a force disturbance at boundaries due to the surface effect.

Based on an infinitesimal element, the virtual work method yields the surface-induced traction directly related to the surface energy density (Chen and Yao, 2014)

$$\boldsymbol{\gamma}_t = \nabla_s\phi,\ \gamma_n\boldsymbol{n} = \phi\left(\frac{1}{R_1}+\frac{1}{R_2}\right)\boldsymbol{n} = \phi(\boldsymbol{n}\cdot\nabla_s)\boldsymbol{n} \tag{3}$$

where ∇_s is a surface gradient operator, ϕ is the Eulerian surface energy density in the current configuration, R_1 and R_2 are two principal radius of curvature of a curved surface.

Combining Eqs. (2) and (3) and using the relationship between the Eulerian surface energy density ϕ and the Lagrangian surface energy density ϕ_0 in the reference configuration $\phi = \phi_0/J_s$, where J_s is a Jacobean determinant characterizing the surface deformation from a reference configuration to a current one, yield the equilibrium equation and stress boundary conditions

$$\begin{cases} \boldsymbol{\sigma}\cdot\nabla + \boldsymbol{f} = 0 (\text{in} V - S) \\ \boldsymbol{n}\cdot\boldsymbol{\sigma}\cdot\boldsymbol{n} = \boldsymbol{p}\cdot\boldsymbol{n} - \phi_0(\boldsymbol{n}\cdot\nabla_s)/J_s \quad (\text{on } S) \\ (\boldsymbol{I}-\boldsymbol{n}\otimes\boldsymbol{n})\cdot\boldsymbol{\sigma}\cdot\boldsymbol{n} = (\boldsymbol{I}-\boldsymbol{n}\otimes\boldsymbol{n}) \\ \quad\cdot\boldsymbol{p} + \phi_0(\nabla_s J_s)/J_s^2 - (\nabla_s\phi_0)/J_s \quad (\text{on } S) \end{cases} \tag{4}$$

The Lagrangian surface energy density ϕ_0 in the reference configuration can be divided into a structural part ϕ_0^{stru} related to the surface strain energy and a chemical part ϕ_0^{chem} originating from the surface dangling-bond energy

$$\phi_0 = \phi_0^{stru} + \phi_0^{chem} \tag{5}$$

where

$$\begin{aligned} \phi_0^{stru} &= \frac{E_b}{2\sin\beta}\sum_{i=1}^{2} a_{0i}\eta_i\left\{\left[3+(\lambda_i+\lambda_i\varepsilon_{si})^{-m}-3(\lambda_i+\lambda_i\varepsilon_{si})\right]\right. \\ &\quad\left.\cdot\left[\lambda_i^2\varepsilon_{si}^2+(\lambda_i-1)^2+2\lambda_i(\lambda_i-1)\varepsilon_{si}\right]\right\} \\ \phi_0^{chem} &= \phi_{0b}\left(1-w_1\frac{D_0}{D}\right), \quad \eta_1 = a_{01}/a_{02}, \quad \eta_2 = a_{02}/a_{01} \end{aligned} \tag{6}$$

Here, ϕ_{0b} is the surface energy density of a bulk material (address as the bulk surface energy density in this paper), D_0 is a critical size ($D_0 = 3d_a$ for nanoparticles, nanowires and $2d_a$ for nanofilms, where d_a is the atomic diameter). D is a characteristic length of nanomaterials or nanostructures (e.g., thickness, diameter, etc.). w_1 is a parameter governing the size-dependent behavior of ϕ_0^{chem}. E_b is the Young's modulus of a bulk material (addressed as the bulk Young's modulus in this paper), $\lambda_i = a_{ri}/a_{0i}$ denotes the surface relaxation parameter, $\varepsilon_{si} = (a_i - a_{ri})/a_{ri}$ is defined as the surface strain induced only by the external loading; m is a parameter describing the dependence of bond lengths on the binding energy ($m = 4$ for alloys or compounds and $m = 1$ for pure metals). Details can be found in Chen and Yao (2014).

The most important difference between our theory and the existing surface energy theories (Gurtin and Murdoch, 1975; Steigmann and Ogden, 1997; Huang and Wang, 2006; Huang and Sun, 2007; Huang, 2010; Huang and Wang, 2010; Chhapadia et al., 2011; Gao et al., 2014b; Gao et al., 2017) is the boundary condition. A surface induced traction due to surface effect in nanomaterials is introduced in the boundary condition of both the previous surface energy theories and ours. In the previous theories, the surface induced traction is related to the surface stress, which obeys a surface elastic constitutive equation. In our model, we establish a relation between the surface energy density and the surface induced traction. As a result, the surface stress in the existing theories would depend on the surface elastic constants. However, with the help of Nix and Gao (1998), Sun (2003), Jiang and Lu (2008) and Ouyang et al. (2009), we derive a new expression of surface energy density from an atomistic perspective, as shown in Eq. (6). Two material parameters, i.e., the bulk surface energy density and surface relaxation parameter, are adopted to characterize the surface effect, instead of the surface elastic constants. Both effects of surface residual stress induced by surface relaxation and the elastic stress induced by an external loading are included in the surface energy density without the introduction of surface elastic constants.

3. Plane strain contact problems with surface effect

Similar to the classical contact mechanics (Johnson, 1987) and contact models considering surface effect (Long et al., 2012; Gao et al., 2013), three typical plane strain contact problems symmetric about z axis are studied with surface effect in the present paper, including an elastic half space subjected to a uniformly distributed load (Boussinesq problem), a rigid flat punch and a cylindrical one, respectively, as shown in Fig. 2. The contact width is a. The origin O of a Cartesian coordinate system xOz is located at the center of the contact zone $-a \le x \le a$, with x axis along the initially flat surface and z axis perpendicular to the surface. The deformation in the out-of-plane direction (y axis) is neglected due to a plane strain assumption.

3.1. Basic equations

The equilibrium equations of a plane-strain contact problem shown in Fig. 2 are as follows

$$\frac{\partial\sigma_x}{\partial x}+\frac{\partial\tau_{xz}}{\partial z}=0,\ \frac{\partial\tau_{xz}}{\partial x}+\frac{\partial\sigma_z}{\partial z}=0 \tag{7}$$

The normal strains ε_x, ε_z, and the shear strain γ_{xz} can be written as

$$\varepsilon_x = \frac{\partial u}{\partial x},\ \varepsilon_z = \frac{\partial w}{\partial z},\ \gamma_{xz} = \frac{\partial u}{\partial z}+\frac{\partial w}{\partial x} \tag{8}$$

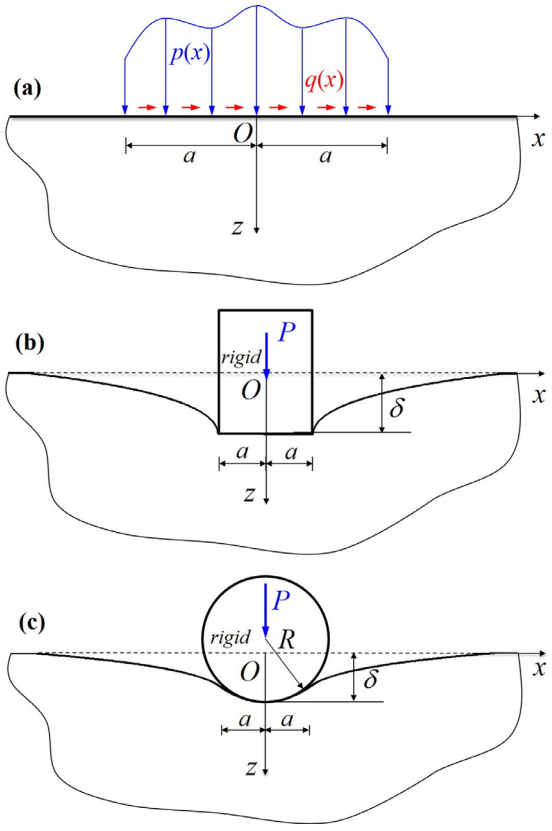

Fig. 2. Schematic of three plane strain contact problems. (a) an elastic half space subjected to uniformly tangential and normal loads; (b) a semi-infinite elastic substrate indented by a rigid flat-ended punch and (c) a Hertzian contact problem with a rigid cylindrical punch.

where u and w are displacements in the x-axis and z-axis directions, respectively.

The constitutive equations of the elastic half space are

$$\varepsilon_x = \frac{1}{2\mu}[(1-\nu)\sigma_x - \nu\sigma_z],\ \varepsilon_z = \frac{1}{2\mu}[(1-\nu)\sigma_z - \nu\sigma_x],\ \gamma_{xz} = \frac{\tau_{xz}}{\mu} \tag{9}$$

where μ and ν are the bulk shear modulus and Poisson's ratio of the half space.

Considering the surface effect leads to an additional surface-induced traction at the contact surface as shown in Eq. (2), in addition to the externally-applied load. The stress boundary conditions at the contact surface can be written as

$$\begin{cases} \sigma_z|_{z=0} + p(x) = -\gamma_n \\ \tau_{xz}|_{z=0} + q(x) = \gamma_x \end{cases} \tag{10}$$

where $p(x)$ and $q(x)$ represent the normal and tangential components of the externally-applied traction, respectively. In this paper, we assume that $p(x)$ is symmetric with respect to z-axis and $q(x)=0$ for the three contact models.

According to Eq. (3) and $\phi = \phi_0/J_s$, the surface-induced traction can be directly formulated as a function of the Lagrangian surface energy density ϕ_0,

$$\gamma_x = \frac{1}{J_s}\frac{\partial\phi_0}{\partial x} - \frac{\phi_0}{J_s^2}\frac{\partial J_s}{\partial x}\bigg|_{z=0},\ \gamma_n = \frac{\phi_0}{J_s}\frac{\partial^2 w}{\partial x^2}\bigg|_{z=0} \tag{11}$$

The general formula of ϕ_0 has been given in Eqs. (5) and (6). For simplicity, we consider xOy as a (100) surface, which has an equal atom spacing in both bond directions. For a semi-infinite elastic substrate, surface relaxation in both bond directions vanishes, i.e., $\lambda_1 = \lambda_2 \approx 1$ (Zhang et al., 2014) and the chemical surface energy density is equal to the surface energy density of a bulk solid due to a large characteristic length D, i.e., $\phi_0^{chem} = \phi_{0b}$. The surface strain ε_{si} $(i=1, 2)$ in both bond directions equals $\varepsilon_x/2$ for a (100) surface (Yao and Chen, 2015, 2016b). Using the technique of Taylor's expansion and ignoring the high-order strain terms ($n > 2$), Eq. (5) can be written as

$$\phi_0 \approx \phi_{0b} + \frac{\sqrt{2}E_b a_0}{8}\varepsilon_x^2\bigg|_{z=0} \tag{12}$$

where a_0 denotes the lattice constant of a bulk material. The strain-dependent surface energy density ϕ_0 has been derived as shown in Eq. (12), which is mainly applicable for materials with an idealized crystal structure, such as metals, alloys and so on.

Combining Eqs. (11) and (12) and noting that $J_s = \lambda^2(1+\varepsilon_x/2)^2$ yield

$$\begin{cases} \sigma_z|_{z=0} + p(x) = -\phi_{0b}(1-\varepsilon_x)\frac{\partial^2 w}{\partial x^2}\big|_{z=0} \\ \tau_{xz}|_{z=0} = -\phi_{0b}(1-\chi\varepsilon_x)\frac{\partial^2 u}{\partial x^2}\big|_{z=0} \end{cases} \tag{13}$$

where $\chi = 2 + \sqrt{2}E_b a_0/(4\phi_{0b})$ is a dimensionless parameter related to the material properties. Under the infinitesimal deformation condition, the normal strain $\varepsilon_x = \partial u/\partial x$ is much less than 1. Moreover, when the surface effect is considered, ε_x should be smaller than its counterpart ε_x^c obtained by classical contact model (Gao et al., 2013), while the latter is already a very small quantity only considering the normal pressure $p(x)$ (Johnson, 1987). Therefore, the strain terms ε_x and $\chi\varepsilon_x$ in Eq. (13) could be approximately omitted, which leads to

$$\begin{cases} \sigma_z|_{z=0} + p(x) = -\phi_{0b}\frac{\partial^2 w}{\partial x^2}\big|_{z=0} \\ \tau_{xz}|_{z=0} = -\phi_{0b}\frac{\partial^2 u}{\partial x^2}\big|_{z=0} \end{cases} \tag{14}$$

Comparing with the classical contact mechanics (Johnson, 1987) shows that the surface energy density of the indented bulk material is involved in the stress boundary conditions in order to characterize the surface effect in nano-indentation. Combining Eqs. (7)–(9) and Eq. (14) results in a boundary-value problem.

3.2. General solutions

Using the stress function method and the Fourier transform technique with respect to x leads to the integral solutions of stress and displacement fields (Selvadurai, 2000)

$$\begin{cases} \sigma_x = \dfrac{\partial^2 U(x,z)}{\partial z^2} = \dfrac{1}{\sqrt{2\pi}}\int_{-\infty}^{\infty}\dfrac{\partial^2\tilde{U}}{\partial z^2}e^{-i\xi x}d\xi \\ \sigma_z = \dfrac{\partial^2 U(x,z)}{\partial x^2} = -\dfrac{1}{\sqrt{2\pi}}\int_{-\infty}^{\infty}\xi^2\tilde{U}e^{-i\xi x}d\xi \\ \tau_{xz} = -\dfrac{\partial^2 U(x,z)}{\partial x\partial z} = \dfrac{i}{\sqrt{2\pi}}\int_{-\infty}^{\infty}\xi\dfrac{\partial\tilde{U}}{\partial z}e^{-i\xi x}d\xi \end{cases} \tag{15}$$

and

$$\begin{cases} u = \dfrac{i}{2\sqrt{2\pi}\mu}\int_{-\infty}^{\infty}\left[(1-\nu)\dfrac{\partial^2\tilde{U}}{\partial z^2} + \nu\xi^2\tilde{U}\right]\dfrac{e^{-i\xi x}}{\xi}d\xi + C_1 \\ w = \dfrac{1}{2\sqrt{2\pi}\mu}\int_{-\infty}^{\infty}\left[(1-\nu)\dfrac{\partial^3\tilde{U}}{\partial z^3} - (2-\nu)\xi^2\dfrac{\partial\tilde{U}}{\partial z}\right]\dfrac{e^{-i\xi x}}{\xi^2}d\xi + C_2 \end{cases} \tag{16}$$

where C_1 and C_2 are integral constants. $\tilde{U}(\xi, z)$ is the Fourier transformation of the stress function $U(x, z)$ with respect to x, which satisfies the following form

$$\tilde{U}(\xi, z) = (A + Bz)e^{-|\xi|z} \tag{17}$$

where A and B are functions of ξ.

Substituting Eqs. (15)–(17) into Eq. (14) yields

$$\begin{cases} A = \dfrac{4[1+(1-\nu)l|\xi|]}{\xi^2[4+8(1-\nu)l|\xi|+(3-4\nu)l^2\xi^2]}\tilde{p}(\xi) \\ B = \dfrac{2\left(2|\xi|+l\xi^2\right)}{\xi^2[4+8(1-\nu)l|\xi|+(3-4\nu)l^2\xi^2]}\tilde{p}(\xi) \end{cases} \tag{18}$$

in which $\tilde{p}(\xi)$ is the Fourier transformation of $p(x)$. l is an intrinsic length scale related to the surface effect, which is defined as a ratio of the bulk surface energy density to the bulk shear modulus, i.e.,

$$l = \frac{\phi_{0b}}{\mu} \tag{19}$$

In our model, the effect of surface relaxation of a semi-infinite substrate tends to vanish (very weak), which is actually reasonable. Thus, the bulk surface energy density serves as a unique material parameter to characterize the surface effect, instead of the surface elastic constant and surface tension used in the other theoretical models (Gao et al., 2013; Gao et al., 2014a). As a result, only one length scale related to the bulk surface energy density is involved in such a semi-infinite half space problem, in contrast to the two length scales associated with surface tension and surface elastic constant in existing models for nano-scale contact problems (Gao et al., 2013; Gao et al., 2014a).

Then, combining Eqs. (15)–(18) yields

$$\begin{cases} \sigma_x = -\sqrt{\dfrac{2}{\pi}}\int_0^\infty \left\{\dfrac{[4(1+\nu l\xi)-2(2+l\xi)\xi z]\cos(\xi x)}{4+8(1-\nu)l\xi+(3-4\nu)l^2\xi^2}\tilde{p}(\xi)\right\}e^{-\xi z}d\xi \\ \sigma_z = -\sqrt{\dfrac{2}{\pi}}\int_0^\infty \left\{\dfrac{2[2(1+l\xi-\nu l\xi)+(2+l\xi)\xi z]\cos(\xi x)}{4+8(1-\nu)l\xi+(3-4\nu)l^2\xi^2}\tilde{p}(\xi)\right\}e^{-\xi z}d\xi \\ \tau_{xz} = -\sqrt{\dfrac{2}{\pi}}\int_0^\infty \left\{\dfrac{2[(1-2\nu)l\xi+(2+l\xi)\xi z]\sin(\xi x)}{4+8(1-\nu)l\xi+(3-4\nu)l^2\xi^2}\tilde{p}(\xi)\right\}e^{-\xi z}d\xi \end{cases} \tag{20}$$

and

$$\begin{cases} u = \dfrac{1}{\mu\sqrt{2\pi}}\int_0^\infty \left\{\dfrac{[4(-1+2\nu)+2(2+l\xi)\xi z]\sin(\xi x)}{\xi[4+8(1-\nu)l\xi+(3-4\nu)l^2\xi^2]}\tilde{p}(\xi)\right\}e^{-\xi z}d\xi + C_1 \\ w = \dfrac{1}{\mu\sqrt{2\pi}}\int_0^\infty \left\{\dfrac{2[4(1-\nu)+l\xi(3-4\nu)+(2+l\xi)\xi z]\cos(\xi x)}{\xi[4+8(1-\nu)l\xi+(3-4\nu)l^2\xi^2]}\tilde{p}(\xi)\right\}e^{-\xi z}d\xi + C_2 \end{cases} \tag{21}$$

Since all the three contact models are symmetric with respect to z-axis as shown in Fig. 2, we have $u(0, z)=0$. Meanwhile, we define the vertical displacement $w(r_0 a, z)=0$, where r_0 is taken as a finite value ($r_0 \geq 5$) (Gao et al., 2013). These two displacement boundary conditions can be used to determine C_1 and C_2.

Let $\xi = t/a$, $x = x'a$, $z = z'a$, $l = l_r a$. Eqs. (20) and (21) become

$$\begin{cases} \sigma_x(x', z') = -\sqrt{\dfrac{2}{\pi}}\int_0^\infty \dfrac{4(1+\nu l_r t)-2(2+l_r t)tz'}{4+8(1-\nu)l_r t+(3-4\nu)l_r^2 t^2}\dfrac{\tilde{p}(t/a)}{a}\cos(tx')e^{-tz'}dt \\ \sigma_z(x', z') = -\sqrt{\dfrac{2}{\pi}}\int_0^\infty \dfrac{2\left[2(1+l_r t-\nu l_r t)+(2+l_r t)tz'\right]}{4+8(1-\nu)l_r t+(3-4\nu)l_r^2 t^2}\dfrac{\tilde{p}(t/a)}{a}\cos(tx')e^{-tz'}dt \\ \tau_{xz}(x', z') = -\sqrt{\dfrac{2}{\pi}}\int_0^\infty \dfrac{2\left[(1-2\nu)l_r t+(2+l_r t)tz'\right]}{4+8(1-\nu)l_r t+(3-4\nu)l_r^2 t^2}\dfrac{\tilde{p}(t/a)}{a}\sin(tx')e^{-tz'}dt \end{cases} \tag{22}$$

$$\begin{cases} u(x', z') = \dfrac{1}{\mu\sqrt{2\pi}}\int_0^\infty \left[\dfrac{4(-1+2\nu)+2(2+l_r t)tz'}{t\left[4+8(1-\nu)l_r t+(3-4\nu)l_r^2 t^2\right]}\cdot \right. \\ \left. \tilde{p}(t/a)\sin(tx')e^{-tz'}\right]dt \\ w(x', z') = \dfrac{2}{\mu\sqrt{2\pi}}\int_0^\infty \left\{\dfrac{4(1-\nu)+(3-4\nu)l_r t+(2+l_r t)tz'}{t\left[4+8(1-\nu)l_r t+(3-4\nu)l_r^2 t^2\right]}\cdot \right. \\ \left. \tilde{p}(t/a)\left[\cos(tx')-\cos(r_0 t)\right]e^{-tz'}\right\}dt \end{cases} \tag{23}$$

in which the Fourier transformation of the normal pressure $p(x)$ satisfies

$$\tilde{p}(t/a) = \frac{a}{\sqrt{2\pi}}\int_{-1}^{1} p(a\eta')\cos(t\eta')d\eta', \quad \eta' = \eta/a \tag{24}$$

It is interesting to find that only the bulk surface energy density of the indented material is involved in Eqs. (22) and (23) to characterize the surface effect in contact problems in contrast to the commonly-used surface residual stress and surface elastic constants (Wang and Feng, 2007; Long et al., 2012; Gao et al., 2013).

(a) For a Boussinesq problem as shown in Fig. 2(a), the elastic half space is subjected to a uniform pressure, i.e., $p(x)=p_0$, then the Fourier transformation in Eq. (24) is

$$\tilde{p}(t/a) = p_0 a\sqrt{\frac{2}{\pi}}\frac{\sin t}{t} \tag{25}$$

with which the stresses and displacements can be obtained.

(b) For a semi-infinite elastic substrate indented by a rigid punch as shown in Fig. 2(b) and 2(c), the normal pressure $p(x)$ at the contact surface is unknown in advance. Substituting Eq. (24) directly into Eqs. (22) and (23) yields the stresses and displacements at the contact surface ($z=0$)

$$\begin{cases} \sigma_x(x', 0) = -\dfrac{1}{\pi}\int_{-1}^{1}\left[-\mathrm{H}_2(x', \eta', l_r, b_1)+\dfrac{3}{3-4\nu}\mathrm{H}_2(x', \eta', l_r, b_2)\right]p(a\eta')d\eta' \\ \sigma_z(x', 0) = -\dfrac{1}{\pi}\int_{-1}^{1}\left[\mathrm{H}_2(x', \eta', l_r, b_1)+\dfrac{1}{3-4\nu}\mathrm{H}_2(x', \eta', l_r, b_2)\right]p(a\eta')d\eta' \\ \tau_{xz}(x', 0) = -\dfrac{1}{\pi}\int_{-1}^{1}\left[\mathrm{H}_1(x', \eta', l_r, b_1)-\dfrac{1}{3-4\nu}\mathrm{H}_1(x', \eta', l_r, b_2)\right]p(a\eta')d\eta' \end{cases} \tag{26}$$

$$\begin{cases} u(x', 0) = -\dfrac{al_r}{4\mu\pi}\int_{-1}^{1}\left[\begin{array}{l}\mathrm{H}_1(x', \eta', l_r, b_1)-(3-4\nu)\mathrm{H}_1(x', \eta', l_r, b_2) \\ +2(1-2\nu)\mathrm{H}_3(x', \eta', l_r)\end{array}\right]p(a\eta')d\eta' \\ w(x', 0) = \dfrac{al_r}{4\mu\pi}\int_{-1}^{1}\left[\begin{array}{l}-\mathrm{H}_2(x', \eta', l_r, b_1)-(3-4\nu)\mathrm{H}_2(x', \eta', l_r, b_2) \\ +\mathrm{H}_5(r_0, \eta', l_r, b_1)+(3-4\nu)\mathrm{H}_5(r_0, \eta', l_r, b_2) \\ +4(1-\nu)\mathrm{H}_4(x', \eta', l_r)\end{array}\right]p(a\eta')d\eta' \end{cases} \tag{27}$$

where

$$\begin{aligned} \mathrm{H}_1(x', \eta', l_r, b) &= \int_0^\infty \frac{\sin\left[t(x'-\eta')\right]}{l_r t+b}dt \\ &= \frac{1}{l_r}\left[\frac{\pi}{2}sgn(\varpi)\cos(\varpi)-\cos(\varpi)Si(\varpi)+\sin(\varpi)Ci(|\varpi|)\right] \\ \mathrm{H}_2(x', \eta', l_r, b) &= \int_0^\infty \frac{\cos\left[t(x'-\eta')\right]}{l_r t+b}dt \\ &= \frac{1}{l_r}\left[\frac{\pi}{2}\sin(|\varpi|)-\cos(\varpi)Ci(|\varpi|)-\sin(\varpi)Si(\varpi)\right] \\ \mathrm{H}_3(x', \eta', l_r) &= \mathrm{sgn}(\varpi)\frac{\pi}{2l_r},\ \mathrm{H}_4(x', \eta', l_r) = \frac{1}{l_r}\ln\left(\left|\frac{\varpi_0}{\varpi}\right|\right) \\ \mathrm{H}_5(r_0, \eta', l_r, b) &= \int_0^\infty \frac{\cos\left[t(r_0-\eta')\right]}{l_r t+b}dt \\ &= \frac{1}{l_r}\left[\frac{\pi}{2}\sin(|\varpi_0|)-\cos(\varpi_0)Ci(|\varpi_0|)-\sin(\varpi_0)Si(\varpi_0)\right] \\ \varpi &= \frac{x'-\eta'}{l_r}b,\ \varpi_0 = \frac{r_0-\eta'}{l_r}b,\ b = \{b_1 = 2b_2 = 2/(3-4\nu) \\ Si(x) &= \int_0^x \frac{\sin\chi}{\chi}d\chi\ for -\infty < x < \infty \\ Ci(x) &= -\int_x^\infty \frac{\cos\chi}{\chi}d\chi\ for x > 0 \end{aligned} \tag{28}$$

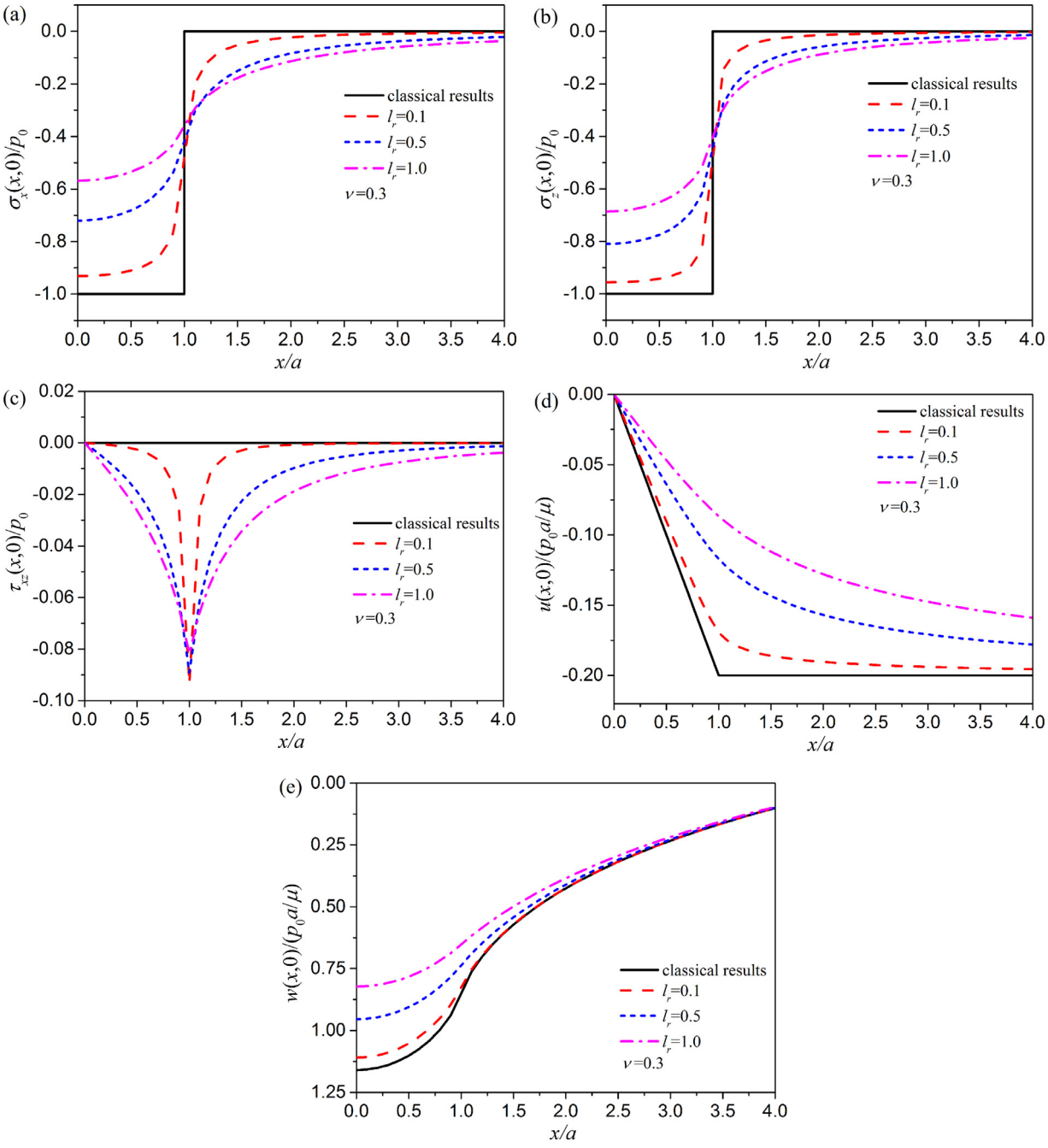

Fig. 3. Distributions of the stresses and displacements at the contact surface in the model of an elastic half-space subjected to a uniform pressure. (a) for the normal stress σ_x; (b) for the normal stress σ_z; (c) for the shear stress τ_{xz}; (d) for the tangential displacement u and (e) for the normal displacement w.

3.3. Solutions of an elastic half space under uniform pressure

Substituting Eq. (25) into Eqs. (22) and (23) yields the stress and displacement fields for the Boussinesq problem as shown in Fig. 2(a),

$$\begin{cases} \sigma_x(x',z') = -\dfrac{2p_0}{\pi}\int_0^\infty \dfrac{4(1+\nu l_r t)-2(2+l_r t)tz'}{4+8(1-\nu)l_r t+(3-4\nu)l_r^2t^2}\dfrac{\sin t}{t}\cos(tx')e^{-tz'}dt \\ \sigma_z(x',z') = -\dfrac{2p_0}{\pi}\int_0^\infty \dfrac{2\left[2(1+l_r t-\nu l_r t)+(2+l_r t)tz'\right]}{4+8(1-\nu)l_r t+(3-4\nu)l_r^2t^2}\dfrac{\sin t}{t}\cos(tx')e^{-tz'}dt \\ \tau_{xz}(x',z') = -\dfrac{2p_0}{\pi}\int_0^\infty \dfrac{2\left[(1-2\nu)l_r t+(2+l_r t)tz'\right]}{4+8(1-\nu)l_r t+(3-4\nu)l_r^2t^2}\dfrac{\sin t}{t}\sin(tx')e^{-tz'}dt \end{cases} \tag{29}$$

$$\begin{cases} u(x',z') = \dfrac{p_0a}{\mu\pi}\int_0^\infty \dfrac{4(-1+2\nu)+2(2+l_r t)tz'}{4+8(1-\nu)l_r t+(3-4\nu)l_r^2t^2}\dfrac{\sin t}{t^2}\sin(tx')e^{-tz'}dt \\ w(x',z') = \dfrac{2p_0a}{\mu\pi}\int_0^\infty \left[\dfrac{4(1-\nu)+(3-4\nu)l_r t+(2+l_r t)tz'}{4+8(1-\nu)l_r t+(3-4\nu)l_r^2t^2}\dfrac{\sin t}{t^2}\cdot \left[\cos(tx')-\cos(r_0 t)\right]e^{-tz'}\right]dt \end{cases} \tag{30}$$

3.4. Solutions of a semi-infinite substrate punched by a rigid flat indenter

As for a semi-infinite elastic substrate indented by a rigid flat-ended punch with a resultant force P along the z-direction,

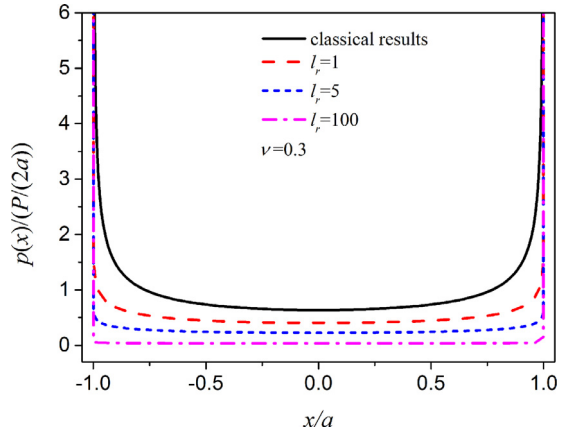

Fig. 4. Distribution of the normal pressure in the contact area of a semi-infinite elastic substrate indented by a rigid flat-ended punch.

in a previous study considering surface effect, a function $p(x) = P/(\pi\sqrt{a^2 - x^2})$was used to represent the distribution of the normal pressure at the contact surface (Gao et al., 2013), which is actually a result obtained by the classical contact mechanics without surface effect (Johnson, 1987). In a contact model considering surface effect, the normal pressure at the contact surface should be an unknown quantity in advance. For a semi-infinite substrate punched by a rigid flat indenter, the normal pressure $p(x)$ at the contact surface should be obtained using the following displacement boundary condition,

$$w(x,0) = \delta = const, \ (|x| \le a) \tag{31}$$

where δ denotes the indent depth.

Differentiating Eq. (31) with respect to x leads to

$$\frac{\partial w(x,0)}{\partial x} = 0, \ (|x| \le a) \tag{32}$$

Combining Eqs. (23), (28) and (32) yields

$$-\frac{1}{2\mu\pi}\int_{-1}^{1}\left[\mathrm{H}_1\left(x',\eta',l_r,b_1\right) + \mathrm{H}_1\left(x',\eta',l_r,b_2\right)\right]p(a\eta')d\eta' = 0 \tag{33}$$

In addition, the relation between the resultant force P and the normal pressure satisfies

$$\frac{1}{\pi}\int_{-1}^{1} p\left(a\eta'\right)d\eta' = \frac{P}{\pi a} \tag{34}$$

Then, with a given external load P and a punch width a, the contact pressure $p(x)$ can be determined based on Eqs. (33) and (34). According to the numerical method provided by Erdogan and Gupta (1972), we transform Eqs. (33) and (34) to a linear algebraic equation as

$$\mathbf{Bp} = \mathbf{f} \tag{35}$$

in which

$$\mathbf{B} = \left[\begin{matrix}[b_{mk}]\\ [b_{nk}]\end{matrix}\right], b_{mk} = \frac{1}{n}\left[\mathrm{H}_1\left(x'_m,\eta'_k,l_r,b_1\right) + \mathrm{H}_1\left(x'_m,\eta'_k,l_r,b_2\right)\right]\sqrt{1-(\eta'_k)^2}$$

$$b_{nk} = \frac{1}{n}\sqrt{1-(\eta'_k)^2}, \mathbf{p} = \left[p\left(a\eta'_1\right),\cdots p\left(a\eta'_k\right),\cdots,p\left(a\eta'_n\right)\right]^T$$

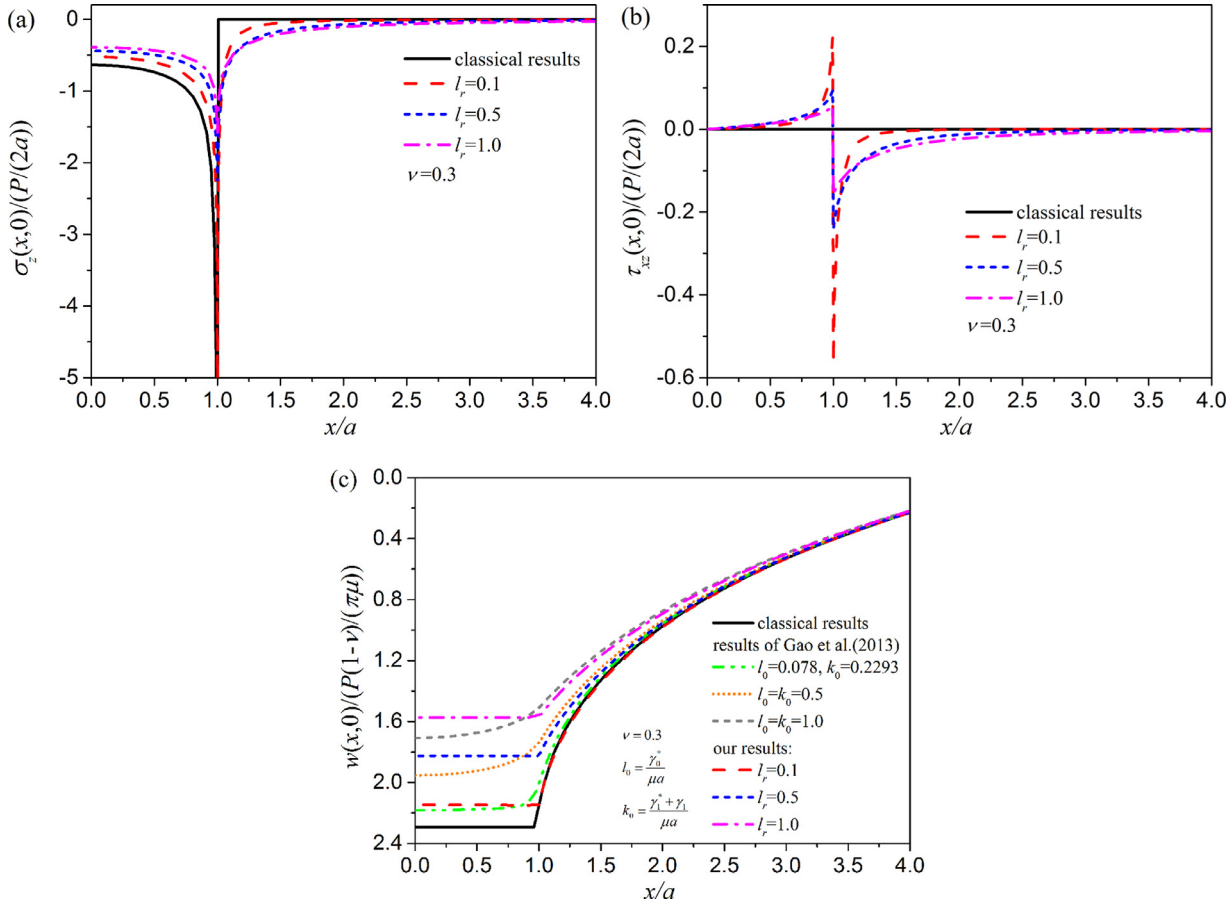

Fig. 5. Distributions of the stresses and displacements at the contact surface in the model of a semi-infinite elastic substrate indented by a rigid flat-ended punch. (a) for the normal stress σ_z; (b) for the shear stress τ_{xz} and (c) for the normal displacement w compared with the results of Gao et al. (2013).

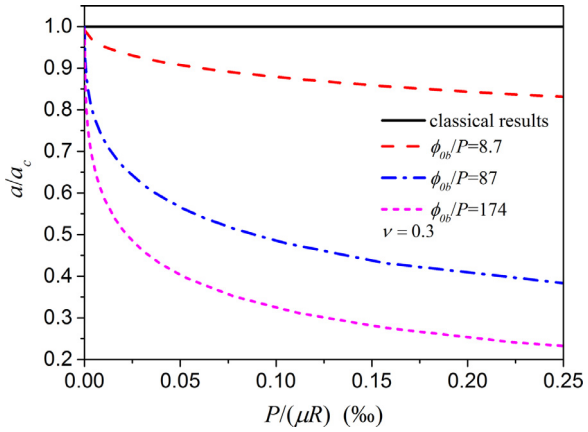

Fig. 6. The normalized contact width a/a_c as a function of the non-dimensional parameter $P/(\mu R)$ in the model of a semi-infinite elastic substrate indented by a rigid cylindrical punch (a Hertzian contact model) with different values of parameter ϕ_{0b}/P.

$$\mathbf{f} = [0, 0, \cdots, 0, P/\pi a]^T, x'_m = \cos\left(\frac{m}{n}\pi\right)(m = 1, \cdots, n-1)$$
$$\eta'_k = \cos\left(\frac{2k-1}{2n}\pi\right)(k = 1, \cdots, n) \tag{36}$$

Thus, $p(x)$ can be obtained by solving Eq. (35), substituting which into Eqs. (26) and (27) yields the stresses and displacements at the contact surface ($z = 0$).

3.5. Solutions of a semi-infinite substrate punched by a rigid cylindrical indenter

As for a semi-infinite substrate punched by a rigid cylinder indenter of radius R with a concentrated force P in the z-direction, the contact width a varies with the external force P. If the surface effect is considered, the classical solution of the normal pressure $p(x) = 2P\sqrt{1-(x/a_c)^2}/(\pi a_c)$ and the contact width $a_c = \sqrt{2(1-\nu)RP/(\pi\mu)}$ obtained in (Johnson, 1987) are no longer valid (Long et al., 2012). The relation between the resultant force P and the normal pressure in Eq. (34) still holds. The displacement boundary condition in the normal direction can be expressed as,

$$\delta - w(x, 0) \approx \frac{x^2}{2R}, (|x| \le a) \tag{37}$$

Differentiating Eq. (37) with respect to x yields

$$\frac{\partial w(x, 0)}{\partial x} = -\frac{x}{R}, (|x| \le a) \tag{38}$$

Combining Eqs. (23), (28) and (38) leads to

$$-\frac{1}{2\mu\pi}\int_{-1}^{1}\left[\mathrm{H}_1\left(x', \eta', l_r, b_1\right) + \mathrm{H}_1\left(x', \eta', l_r, b_2\right)\right]p(a\eta')d\eta' = -\frac{ax'}{R} \tag{39}$$

Similar to Section 3.4, Eqs. (34) and (39) can be written as a linear algebraic equation according to Erdogan and Gupta (1972),

$$\mathbf{Bp} = \mathbf{f}, \mathbf{B} = \begin{bmatrix}[b_{mk}] \\ [b_{nk}]\end{bmatrix},$$
$$b_{mk} = \frac{1}{n}\left[\mathrm{H}_1\left(x'_m, \eta'_k, l_r, b_1\right) + \mathrm{H}_1\left(x'_m, \eta'_k, l_r, b_2\right)\right]\sqrt{1-(\eta'_k)^2}$$
$$b_{nk} = \frac{1}{n}\sqrt{1-(\eta'_k)^2}, \mathbf{p} = \left[p\left(a\eta'_1\right), \cdots p\left(a\eta'_k\right), \cdots, p\left(a\eta'_n\right)\right]^T$$

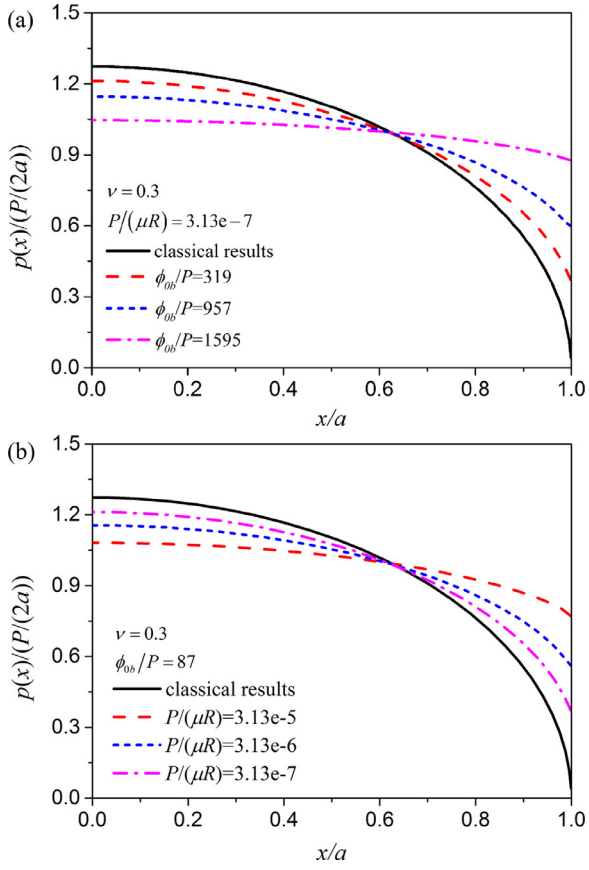

Fig. 7. The normal pressure at the contact surface influenced by different mechanical parameters in the model of a semi-infinite elastic substrate indented by a rigid cylindrical punch. (a) for the parameter ϕ_{0b}/P; (b) for the parameter $P/(\mu R)$.

$$\mathbf{f} = \left[\cdots, \frac{2a\mu}{R}x'_m, \cdots, P/\pi a\right]^T, x'_m = \cos\left(\frac{m}{n}\pi\right)(m = 1, \cdots, n-1)$$
$$\eta'_k = \cos\left(\frac{2k-1}{2n}\pi\right)(k = 1, \cdots, n) \tag{40}$$

Solving Eq. (40) numerically yields the pressure $p(x)$ and the contact width a, substituting which into Eqs. (26) and (27) yields the stresses and displacements at the contact surface ($z = 0$).

4. Results and discussion

Based on the above numerical solutions, the stresses and displacements in three two-dimensional contact models with surface effect are predicted and compared with those obtained by the classical contact mechanics (Johnson, 1987). In this paper, we take $\nu = 0.3$ and $r_0 = 5$.

4.1. Case of an elastic half space subjected to a uniform pressure

Stresses and displacements at the surface of an elastic half space subjected to a uniform pressure can be obtained from Eqs. (29) and (30), which are shown in Fig. 3 with a dimensionless parameter $l_r = \phi_{0b}/(\mu a)$ characterizing the surface effect. It is clearly found from Fig. 3(a) and (b) that the normal stresses in the contact area are obviously smaller than the classical solutions in the contact region, while the ones outside the contact area are larger than the classical solutions (absolute values for compressive stresses). As a result, the surface effect in such a Boussinesq problem leads to a smoother distribution of normal stresses at the surface as

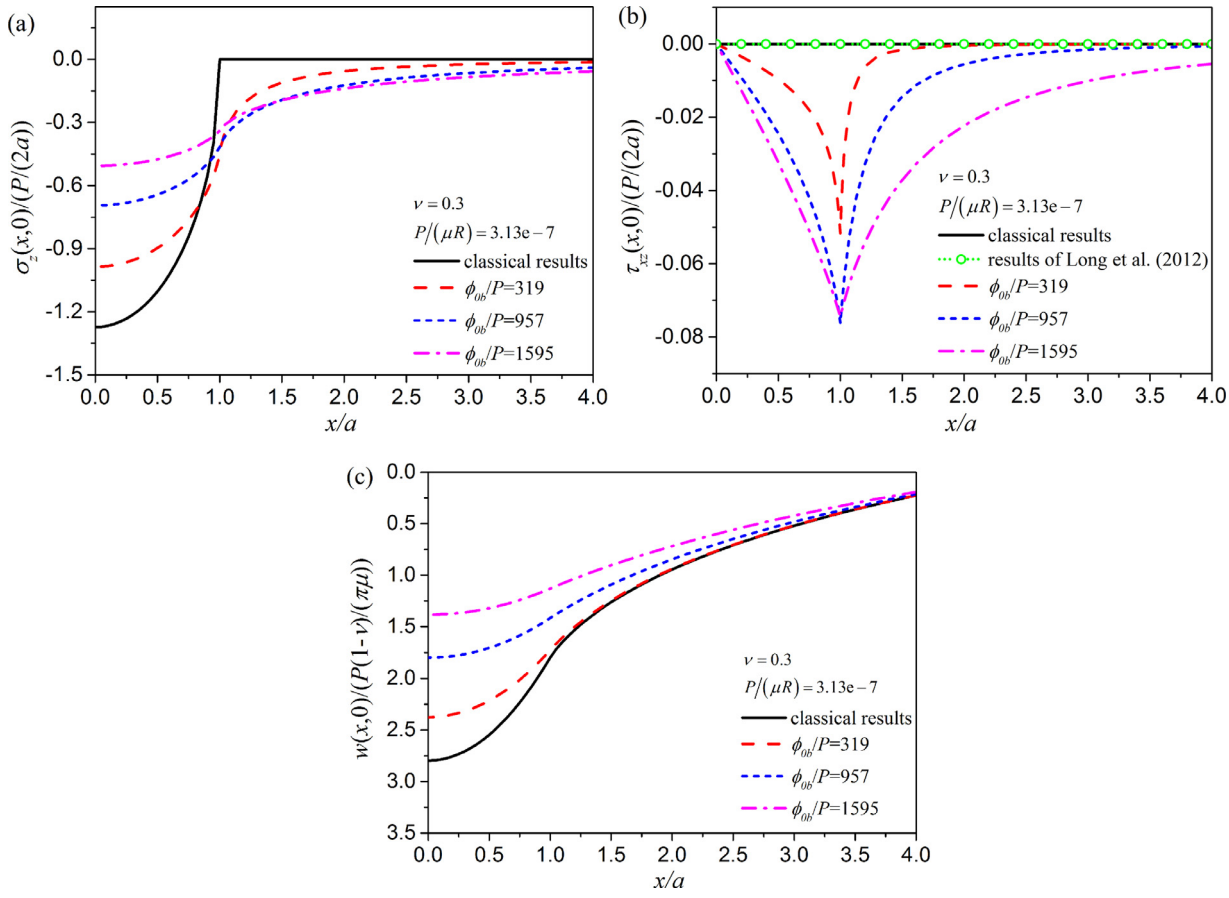

Fig. 8. Distributions of the stresses and displacements at the contact surface in the model of a semi-infinite elastic substrate indented by a rigid cylindrical punch. (a) for the normal stress σ_z; (b) for the shear stress τ_{xz} and (c) for the normal displacement w.

compared to the classical ones, in which an unphysical discontinuous jump exists at the contact edge $|x| = a$. Fig. 3(c) shows a non-zero shear stress at the contact surface in contrast to the zero one predicted by classical contact models, which is essentially due to the action of surface-induced tangential traction. Both the tangential and normal displacements are smaller than their classical counterparts as shown in Fig. 3(d) and 3(e), which indicates a hardening effect due to the surface effect. As the intrinsic length parameter l_r decreases, all the results predicted by the present model approach the classical ones. Meanwhile, Fig. 3(d) shows that the gradient of the tangential displacement with surface effect is smaller than the that of the classical result, which is consistent with the phenomenon revealed by Gao et al. (2013) that the normal strain $\varepsilon_x = \partial u/\partial x$ due to the surface effect is smaller than its classical counterpart $\varepsilon_x^c = -(1-2\nu)p_0/(2\mu)$.

4.2. Case of a semi-infinite substrate punched by a rigid flat indenter

As pointed out in Section 3.4, the normal pressure under a rigid flat punch should no longer follow the classical description $p(x) = P/(\pi\sqrt{a^2-x^2})$ (Johnson, 1987) if the surface effect is considered. The difference is clearly illustrated in Fig. 4. The normal pressure $p(x)$ with surface effect is smaller and more uniform than the classical one, which decreases with an increasing intrinsic length l_r.

The distributions of normal and shear stresses and the normal displacement are presented in Figs. 5(a)–(c). The solutions given by the classical contact mechanics are also shown for comparison. Similar to the Boussinesq case in Section 4.1, the normal stresses with surface effect are smoother than the classical solutions. That is the normal stresses with surface effect are smaller than the classical ones in the contact region, while the absolute values of the normal stresses with surface effect are larger than the classical ones outside the contact area as shown in Fig. 5(a). Furthermore, a non-zero shear stress at the contact surface exists in contrast to a vanishing one in the classical contact solution as shown in Fig. 5(b). When the surface effect is considered, the normal displacement is smoother than the classical solution. That is the absolute values of the displacements with surface effect are smaller than the classical ones. All the results are influenced by the intrinsic length l_r, which characterizes the surface effect. When the intrinsic length decreases, all the terms approach to the classical solutions.

Moreover, Fig. 5(c) shows that the normal displacement in the contact region predicted by the present model keeps a constant, whether the surface effect is considered or not. However, a non-uniformly normal displacement was predicted in Gao et al. (2013) though it is a problem with a rigid flat-ended indenter. It should be due to the simple assumption that the normal pressure $p(x)$ was adopted directly to be the same as the classical solution, i.e., the so-called "elliptic function" (Johnson, 1987), even though the surface effect was considered at the contact surface (Gao et al., 2013). In order to check the applicable range of the elliptical function adopted by Gao et al. (2013), Fig. 5(c) presents the prediction of the normal displacement obtained by Gao et al. (2013) and the present model, in which the increase of the intrinsic length means an enhancement of surface effect (Gao et al., 2013). One can see that the displacement under a flat indenter predicted by Gao et al. (2013) is not a constant and the deviation of the non-uniform displacement from a constant one in the contact region becomes more and more significant with an enhancing surface effect. Comparison of the results obtained by Gao et al. (2013) and the present

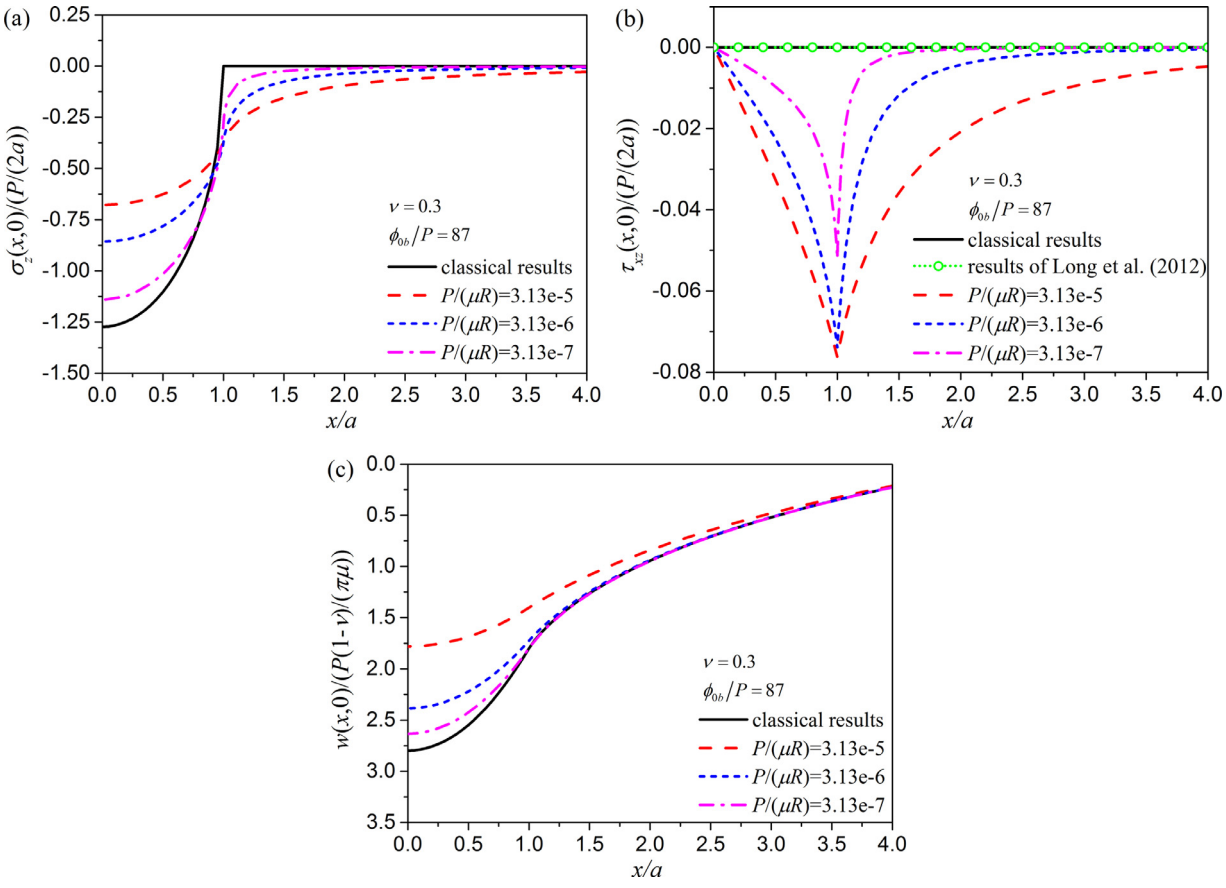

Fig. 9. The effect of the cylindrical punch radius on the distributions of mechanical properties. (a) for the normal stress σ_z; (b) for the shear stress τ_{xz} and (c) for the normal displacement w.

ones shows that the elliptic function may be appropriate to describe the pressure distribution only for the case with a relatively weak surface effect.

4.3. Case of a semi-infinite substrate punched by a rigid cylindrical indenter

As for the plane strain contact model of a semi-infinite substrate punched by a rigid cylindrical indenter, the contact width a should vary with the external force P. A dimensionless ratio ϕ_{0b}/P is adopted to characterize the surface effect instead of the previously adopted non-dimensional parameter $l_r = \phi_{0b}/(\mu a)$. In addition, a non-dimensional parameter $P/(\mu R)$ is also introduced in order to characterize the size effect of cylinder radius.

The normalized contact width a/a_c versus the non-dimensional parameter $P/(\mu R)$ is shown in Fig. 6, where $a_c = \sqrt{2(1-\nu)RP/(\pi\mu)}$ denotes half of the contact width predicted by the classical contact mechanics. It is found that the contact width is influenced significantly by the surface effect. For a fixed parameter ϕ_{0b}/P, the present contact width is smaller than the classical one and decreases with an increasing parameter $P/(\mu R)$. For a fixed parameter $P/(\mu R)$, the present contact width decreases with an increasing ϕ_{0b}/P, which means the larger the bulk surface energy density, the smaller the contact width. In general, surface effect will exhibit a hardening effect on the indented substrate.

Analogous to the previous two cases, the normal pressure $p(x)$ in this case becomes more uniform than the classical solution as shown in Fig. 7(a) and (b). Furthermore, the normal pressure does not vanish at the contact edge $x = \pm a$ in contrast to the classical Hertzian solution, which is due to a non-vanishing surface-induced traction. Figs. 7(a) and (b) also show that $p(x)$ gradually tends to the average value $P/(2a)$ for an increasing ϕ_{0b} or a decreasing R.

Comparisons of the normal stresses and the tangential one as well as the displacements at the contact surface predicted by the present model and the classical solution are shown in Figs. 8 and 9 for a fixed parameter $P/(\mu R)$ and ϕ_{0b}/P, respectively. The variation trends of all the terms in this case are similar to those of the first two cases, when the present results are compared with the classical ones. An increasing bulk surface energy density or a decreasing punch radius should be responsible for the enhanced surface effect. Moreover, it is interesting to note from Figs. 8(b) and 9(b) that the shear stress at contact surface is non-zero though the contact between the substrate and the rigid indenter is assumed to be frictionless, which is different from the zero shear stress predicted by Long et al. (2012) considering the effect of surface tension. This difference is due to the surface-induced tangential traction in the boundary condition of our surface energy model, as shown in Eq. (14), which was not included in classical contact models and the model of Long et al. (2012).

The indentation hardness is further analyzed for the present model, which is defined as $H = P/(2a)$. Normalized indentation hardness H/H_c as a function of the non-dimensional parameter R/l is shown in Fig. 10 for different values of ϕ_{0b}/P, where H_c has a classical definition, $H_c = \sqrt{P\pi\mu/[8(1-\nu)R]}$. Similar to the ISE in micro-mechanics, for a fixed value of ϕ_{0b}/P, the smaller the punch radius (equivalent to a decreasing contact width), the larger the indentation hardness. Furthermore, for a fixed R/l and a determined P, the larger the bulk surface energy density, the larger the pre-

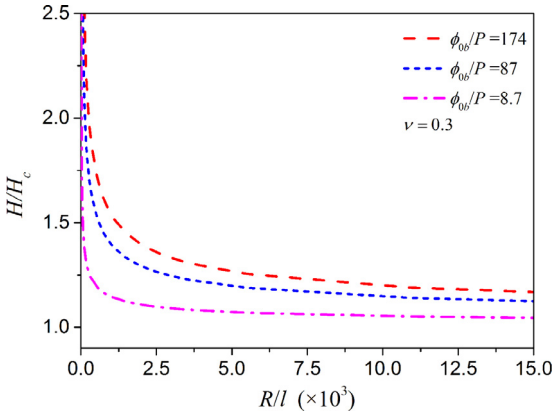

Fig. 10. Normalized indentation hardness H/H_c varying with the non-dimensional parameter R/l in the model of a semi-infinite elastic substrate indented by a plane strain cylindrical punch.

dicted indentation hardness. All these further demonstrate a hardening effect on the substrate due to the surface effect.

5. Conclusions

An elastic theory developed for nanomaterials is adopted in this paper to analyze the surface effect on a semi-infinite substrate's contact behaviors and its indentation hardness. Three two-dimensional models are studied, including an elastic half space under uniformly normal pressure, a semi-infinite substrate punched by a flat-ended indenter as well as a semi-infinite substrate punched by a cylindrical indenter. The contact stresses and the displacements are mainly investigated. It is found that surface effect on the contact behaviors cannot be neglected when the contact width is on the same magnitude with the ratio of the bulk surface energy density to the bulk shear modulus of the indented material. Comparisons of the present theoretical predictions with the classical contact solutions demonstrate that surface effect could not only smoothen and reduce the normal stresses and displacements, but also induce a non-zero shear stress at the contact surface. Moreover, the normal stresses under a rigid flat punch or a cylindrical one as well as the width of the Hertzian contact zone are determined. The former becomes more uniform and the latter shrinks as compared to the corresponding classical predictions. The surface effect can be enhanced by an increasing bulk surface energy density of the indented material or a reducing punch size (contact width). Nano-indentation hardness is also influenced significantly by surface effect of the indented material, which can be improved obviously with a decreasing punch size or external force in comparison with the classical prediction. All the results should be helpful not only for precise measurement of nano-indentation hardness but also for accurate evaluation of surface properties of nanomaterials and nano-devices.

Acknowledgments

The work reported here is supported by NSFC through Grants #11532013, #11372317, #11402270 and the BIT Creative Research Plan.

References

Chen, S.H., Wang, T.C., 2000. A new hardening law for strain gradient plasticity. Acta Mater 48, 3997–4005.
Chen, S.H., Wang, T.C., 2002. A new deformation theory with strain gradient effects. Int. J. Plast 18, 971–995.
Chen, S.H., Yao, Y., 2014. Elastic theory of nanomaterials based on surface-energy density. J. Appl. Mech. 81, 121002.
Chen, T.Y., Chiu, M.S., Weng, C.N., 2006. Derivation of the generalized Young-Laplace equation of curved interfaces in nanoscaled solids. J. Appl. Phys. 100, 074308.
Chhapadia, P., Mohammadi, P., Sharma, P., 2011. Curvature-dependent surface energy and implications for nanostructures. J. Mech. Phys. Solids 59, 2103–2115.
Erdogan, F., Gupta, G., 1972. On the numerical solution of singular integral equations (Singular integral equations numerical solution from Gauss–Chebyshev formulas for mixed boundary value problems). Q Appl Math 29, 525–534.
Feng, G., Nix, W.D., 2004. Indentation size effect in MgO. Scr. Mater. 51, 599–603.
Fleck, N.A., Muller, G.M., Ashby, M.F., Hutchinson, J.W., 1994. Strain gradient plasticity: theory and experiment. Acta Metall. Mater. 42, 475–487.
Gao, X., Hao, F., Fang, D., Huang, Z., 2013. Boussinesq problem with the surface effect and its application to contact mechanics at the nanoscale. Int. J. Solids Struct. 50, 2620–2630.
Gao, X., Hao, F., Huang, Z.P., Fang, D.N., 2014a. Mechanics of adhesive contact at the nanoscale: the effect of surface stress. Int. J. Solids Struct. 51, 566–574.
Gao, X., Huang, Z., Fang, D., 2017. Curvature-dependent interfacial energy and its effects on the elastic properties of nanomaterials. Int. J. Solids Struct. 113, 100–107.
Gao, X., Huang, Z., Qu, J., Fang, D., 2014b. A curvature-dependent interfacial energy-based interface stress theory and its applications to nano-structured materials: (I) General theory. J. Mech. Phys. Solids 66, 59–77.
Gerberich, W., Tymiak, N., Grunlan, J., Horstemeyer, M., Baskes, M., 2002. Interpretations of indentation size effects. J. Appl. Mech. 69, 433–442.
Gurtin, M.E., Murdoch, A.I., 1975. A continuum theory of elastic material surfaces. Arch. Ration. Mech. Anal. 57, 291–323.
Gurtin, M.E., Murdoch, A.I., 1978. Surface stress in solids. Int. J. Solids Struct. 14, 431–440.
Hajji, M., 1978. Indentation of a membrane on an elastic half space. J. Appl. Mech. 45, 320–324.
He, J., Lilley, C.M., 2008. Surface stress effect on bending resonance of nanowires with different boundary conditions. Appl. Phys. Lett. 93, 263108.
Huang, Y., Zhang, F., Hwang, K., Nix, W., Pharr, G., Feng, G., 2006. A model of size effects in nano-indentation. J. Mech. Phys. Solids 54, 1668–1686.
Huang, Z., 2010. Erratum to: size-dependent effective properties of a heterogeneous material with interface energy effect: from finite deformation theory to infinitesimal strain analysis. Acta Mech 215, 363–364.
Huang, Z., Wang, J., 2010. Erratum to: a theory of hyperelasticity of multi-phase media with surface/interface energy effect. Acta Mech 215, 365–366.
Huang, Z.P., Sun, L., 2007. Size-dependent effective properties of a heterogeneous material with interface energy effect: from finite deformation theory to infinitesimal strain analysis. Acta Mech 190, 151–163.
Huang, Z.P., Wang, J., 2006. A theory of hyperelasticity of multi-phase media with surface/interface energy effect. Acta Mech 182, 195–210.
Huang, Z.P., Wang, J.X., 2013. Micromechanics of Nanocomposites With Interface Energy Effect, Handbook of Micromechanics and Nanomechanics. Pan Stanford Publishing.
Jiang, Q., Lu, H., 2008. Size dependent interface energy and its applications. Surf. Sci. Rep. 63, 427–464.
Johnson, K.L., 1987. Contact Mechanics. Cambridge university press.
Koguchi, H., 1996. Stress analysis for nano-scale elastic materials: elastic contact problems considering surface stresses. JSME Int. J. Ser. A Mech. Mater. Eng. 39, 337–345.
Koguchi, H., 2008. Surface green function with surface stresses and surface elasticity using Stroh's formalism. J. Appl. Mech. 75, 061014.
Li, P., Wang, Q., Shi, S., 2011. Differential scheme for the effective elastic properties of nano-particle composites with interface effect. Comput. Mater. Sci. 50, 3230–3237.
Li, X., An, Y.H., Wu, Y.D., Song, Y.C., Chao, Y.J., Chien, C.H., 2007. Microindentation test for assessing the mechanical properties of cartilaginous tissues. J. Biomed. Mater. Res. Part B Appl. Biomater. 80, 25–31.
Long, J., Wang, G., Feng, X., Yu, S., 2012. Two-dimensional Hertzian contact problem with surface tension. Int. J. Solids Struct. 49, 1588–1594.
Long, J., Wang, G., Feng, X.Q., Yu, S., 2016. Effects of surface tension on the adhesive contact between a hard sphere and a soft substrate. Int. J. Solids Struct. 84, 133–138.
Mi, C., Jun, S., Kouris, D.A., Kim, S.Y., 2008. Atomistic calculations of interface elastic properties in noncoherent metallic bilayers. Phys. Rev. B 77, 439–446.
Miller, R.E., Shenoy, V.B., 2000. Size-dependent elastic properties of nanosized structural elements. Nanotechnology 11, 139.
Nix, W.D., Gao, H., 1998. Indentation size effects in crystalline materials: a law for strain gradient plasticity. J. Mech. Phys. Solids 46, 411–425.
Ouyang, G., Wang, C., Yang, G., 2009. Surface energy of nanostructural materials with negative curvature and related size effects. Chem. Rev. 109, 4221–4247.
Rar, A., Pharr, G.M., Oliver, W.C., Karapetian, E., Kalinin, S.V., 2006. Piezoelectric nanoindentation. J. Mater. Res. 21, 552–556.
Selvadurai, A.P., 2000. Partial Differential Equations in Mechanics 2: The Biharmonic Equation, Poisson's Equation. Springer Science & Business Media.
Shenoy, V.B., 2005. Atomistic calculations of elastic properties of metallic FCC crystal surfaces. Phys. Rev. B 71, 094104.
Steigmann, D., Ogden, R., 1997. Plane deformations of elastic solids with intrinsic boundary elasticity. In: Proceedings of the Royal Society of London A: Mathematical, Physical and Engineering Sciences. The Royal Society, pp. 853–877.
Sun, C.Q., 2003. Oxidation electronics: bond–band–barrier correlation and its applications. Prog. Mater. Sci. 48, 521–685.
Voyiadjis, G.Z., Al-Rub, R.K.A., 2005. Gradient plasticity theory with a variable length scale parameter. Int. J. Solids Struct. 42, 3998–4029.

Wang, G., Feng, X., 2007. Effects of surface stresses on contact problems at nanoscale. J. Appl. Phys. 101, 013510.
Wang, G.F., Feng, X.Q., 2009. Timoshenko beam model for buckling and vibration of nanowires with surface effects. J. Phys. D 42, 155411.
Yao, Y., Chen, S., Fang, D., 2017. An interface energy density-based theory considering the coherent interface effect in nanomaterials. J. Mech. Phys. Solids 99, 321–337.
Yao, Y., Chen, S.H., 2015. Surface effect on resonant properties of nanowires predicted by an elastic theory for nanomaterials. J. Appl. Phys. 118, 044303.
Yao, Y., Chen, S.H., 2016a. Buckling behavior of nanowires predicted by a new surface energy density model. Acta Mech 227, 1799–1811.
Yao, Y., Chen, S.H., 2016b. Surface effect in the bending of nanowires. Mech. Mater. 100, 12–21.
Yao, Y., Wei, Y., Chen, S., 2015. Size effect of the surface energy density of nanoparticles. Surf. Sci. 636, 19–24.
Zhang, C., Yao, Y., Chen, S., 2014. Size-dependent surface energy density of typically fcc metallic nanomaterials. Comput. Mater. Sci. 82, 372–377.
Zhang, T.-Y., Xu, W.-H., 2002. Surface effects on nanoindentation. J. Mater. Res. 17, 1715–1720.
Zhao, X., Rajapakse, R., 2009. Analytical solutions for a surface-loaded isotropic elastic layer with surface energy effects. Int. J. Eng Sci 47, 1433–1444.
Zhou, S., Gao, X.-L., 2013. Solutions of half-space and half-plane contact problems based on surface elasticity. Z. Angew. Math. Phys. 64, 145–166.